

Measurement-based Fast Quantum State Stabilization with Deep Reinforcement Learning

Chunxiang Song, Yanan Liu, Daoyi Dong, Hidehiro Yonezawa

Abstract—The stabilization of quantum states is a fundamental problem for realizing various quantum technologies. Measurement-based-feedback strategies have demonstrated powerful performance, and the construction of quantum control signals using measurement information has attracted great interest. However, the interaction between quantum systems and the environment is inevitable, especially when measurements are introduced, which leads to decoherence. To mitigate decoherence, it is desirable to stabilize quantum systems faster, thereby reducing the time of interaction with the environment. In this paper, we utilize information obtained from measurement and apply deep reinforcement learning (DRL) algorithms, without explicitly constructing specific complex measurement-control mappings, to rapidly drive random initial quantum state to the target state. The proposed DRL algorithm has the ability to speed up the convergence to a target state, which shortens the interaction between quantum systems and their environments to protect coherence. Simulations are performed on two-qubit and three-qubit systems, and the results show that our algorithm can successfully stabilize random initial quantum system to the target entangled state, with a convergence time faster than traditional methods such as Lyapunov feedback control. Moreover, it exhibits robustness against imperfect measurements and delays in system evolution.

Index Terms—quantum state stabilization, feedback control, learning control, deep reinforcement learning (DRL)

I. INTRODUCTION

QUANTUM control theory focuses on manipulating quantum systems using external control fields or operations to regulate their behaviors [1]. A significant objective in quantum control is the preparation of target states, particularly quantum entangled states, which serve as vital resources for various quantum applications, including quantum teleportation [2], [3], fast quantum algorithms [3], [4], and quantum computations [5]. Achieving high-fidelity entangled states often involves using classical control methods, with feedback control technology being particularly noteworthy. Quantum systems can be stabilized at target states or spaces through feedback control methods that continuously monitor the system and design feedback controllers based on real-time feedback information. In quantum measurement-based feedback, quantum measurements, while providing valuable information, introduce

stochastic noise, complicating the state preparation process. To address the challenges posed by stochastic nonlinear problems in quantum systems due to measurements, some classical control methods, such as the Lyapunov method [6]–[8], have been applied. However, devising feedback strategies remains a formidable task, given the vast space of possibilities where different responses may be required for each measurement outcome. Moreover, opportunities exist for further enhancing stability and convergence speed.

Recently, quantum learning control, first introduced in [9], has proven potential in addressing various quantum control problems. Its popularity has grown with the incorporation of additional machine learning (ML) algorithms that exhibit excellent optimization performance and promising outcomes. Quantum learning control concerns to apply proper ML algorithms as promising tools for improving quantum system performance [9]–[13], and can offer robust solutions for developing effective quantum control and estimation methods [10]. For instance, the utilization of gradient algorithms in quantum learning control has demonstrated its significance in addressing quantum robust control problems [14]. Another example involves a widely used class of algorithms, evolutionary algorithms (EAs), which gains attention in learning control due to their ability to avoid local optima and their independence from gradient information [1]. Nonetheless, the real-time nature and randomness of measurement feedback control pose challenges, expanding the decision space significantly due to randomness [15]. This randomness makes it almost impossible to reproduce the same measurement trajectory, bringing challenges for EAs to apply control policies from certain sample trajectories to entirely different ones.

Deep reinforcement learning (DRL) emerges as a promising solution to tackle these challenges. Since the introduction of the first DRL algorithm, deep Q-network (DQN) [16], in 2013, and the groundbreaking success of AlphaGo [17] defeating the world champion in the game of Go in 2016, DRL has garnered significant attention. As a ML methodology, DRL employs trial-and-error learning to train intelligent agents to make improved decisions in their environment, aiming to maximize cumulative rewards. The primary step involves the DRL agent engaging with the environment, gathering data and enhancing its policy to optimize decision-making across all states. The process continues iteratively, providing “better” control signals to achieve predefined control objectives [1]. DRL thus has found successful applications in quantum control fields to achieve different control objectives, which include stabilizing quantum states [18]–[22], optimizing high-fidelity quantum gates [23], and cooling a quantum harmonic oscillator [24].

Chunxiang Song is with the School of Engineering and Technology, University of New South Wales, Canberra, ACT 2600, Australia (e-mail: chunxsong@gmail.com).

Yanan Liu is with the School of Engineering, University of Newcastle, Callaghan, NSW 2308, Australia (e-mail: yaananliu@gmail.com).

Daoyi Dong is with the School of Engineering, Australian National University, Canberra, ACT 2601, Australia (e-mail: daoyidong@gmail.com).

Hidehiro Yonezawa is with the Optical Quantum Control Research Team, RIKEN Center for Quantum Computing, 2-1 Hirosawa, Wako, Saitama, 351-0198, Japan (e-mail: hidehiro.yonezawa@riken.jp).

An intriguing avenue of research using DRL in quantum measurement feedback control involves employing measurement results as training data to develop control strategies for quantum systems. For instance, in the context of cooling the system of a particle in a potential well to their ground state, position measurements are employed, and the measured current is directly used as feedback information to train the DRL agent, resulting in a relatively high-fidelity final state [25]. Recent advancements have also proposed the utilization of the density matrix of the quantum state as input for training DRL agents. These agents use fidelity as a reward function, allowing them to generate simple linear control signals for preparing and stabilizing Fock states of the cavity [20], [21].

Our study is motivated by the application of suitable DRL algorithms within feedback loops to exploit information obtained from measurements, thereby achieving predefined objectives. This approach holds the potential to enhance feedback control schemes, leading to a notable reduction in the convergence time to reach target states and exhibiting robustness in the face of uncertainties. In our study, we aim to devise a feedback control scheme based on DRL algorithms to enhance state stabilization, focusing primarily on entangled quantum states. These states present unique challenges due to their geometric symmetries and multi-qubit nature.

To achieve the objectives, we exploit the information derived from quantum measurement as the input signal to train our DRL agent. The agent actively interacts with the quantum system, making control decisions based on the received input. We design a generalized reward function that quantifies the similarity between the current quantum state and the desired target state. This incentivizes the DRL agent to iteratively learn control strategies that maximize rewards, ultimately leading to more effective control strategies for stabilizing entangled quantum states. Our work contributes to the field of quantum information processing and quantum computation, shedding light on the potential of DRL in addressing complex quantum control challenges.

The main contributions of this paper are as follows:

- 1) A DRL algorithm is proposed to achieve the stabilization of given entangled states. We design an effective and versatile reward function based on the distance between the system state and the target state, allowing flexible parameter adjustment for different objectives to enhance the performance of the DRL agent.
- 2) We compare the proposed DRL-based control strategy with the Lyapunov method for Bell state and GHZ state preparation through numerical simulations. The DRL-based control fields achieve a faster stabilization for both target states, which effectively reduces the noise generated during system-environment interactions.
- 3) We analyze the robustness of our DRL scheme under the presence of imperfect measurements and time delays in the feedback loop. The trained DRL agent exhibits remarkable adaptability to uncertainties in the environment, particularly excelling in the pursuit of robust control fields to achieve quantum state stability.

The following is the organization of this paper. Section II briefly introduces the stochastic master equation for quantum

systems under continuous weak measurements. Section III explains in detail the logic and implementation behind DRL. Section IV gives some details of the implementation of DRL in the quantum measurement feedback control. Numerical results are given in Section V. Section VI is the conclusion.

II. QUANTUM SYSTEM DYNAMICS

For a quantum system, its state can be represented by a density matrix ρ defined in the Hilbert space \mathbb{H} . This density matrix exhibits essential properties: Hermitian ($\rho = \rho^\dagger$), trace unity ($\text{Tr}(\rho) = 1$), and positive semi-definite ($\rho \geq 0$). The dynamics of the quantum system may be observed through continuous weak measurements, enabling us to acquire pertinent measurement information for the design of an appropriate feedback controller. The evolution of the quantum trajectory can be described using the stochastic master equation (SME) [15], [26]:

$$d\rho_t = -\frac{i}{\hbar}[H_0 + \sum_{j=1}^M u_j(t)H_j, \rho_t]dt + \kappa_c \mathcal{D}[c]\rho_t dt + \sqrt{\eta_c \kappa_c} \mathcal{H}[c]\rho_t dW, \quad (1)$$

where $i = \sqrt{-1}$, the reduced Planck constant $\hbar = 1$ is used throughout this paper; the Hermitian operator H_0 and H_j ($j = 1, 2, \dots, M$) are the free Hamiltonian and control Hamiltonians, respectively; $u_j(t)$ is a real-valued control signal, which can be interpreted as the strength of the corresponding control Hamiltonians H_j ; κ_c and η_c are measurement strength and efficiency, respectively; dW is a standard Wiener process caused by measurement; the Hermitian operator c is an observable; the superoperators $\mathcal{D}[c]\rho_t$ and $\mathcal{H}[c]\rho_t$ are related to the measurement, e.g., they can describe the disturbance to the system state, and the information gain from the measurement process, respectively [27], and have the following forms:

$$\begin{cases} \mathcal{D}[c]\rho_t = c\rho_t c^\dagger - \frac{1}{2}c^\dagger c\rho_t - \frac{1}{2}\rho_t c^\dagger c, \\ \mathcal{H}[c]\rho_t = c\rho_t + \rho_t c^\dagger - \text{Tr}[(c + c^\dagger)\rho_t]\rho_t. \end{cases} \quad (2)$$

On any given trajectory the corresponding measured current is $I(t) = dy(t)/dt$ [26], [28] where

$$dy(t) = \sqrt{\eta_c \kappa_c} \text{Tr}[(c + c^\dagger)\rho_t]dt + dW. \quad (3)$$

With the measurement result y_t , statistical information on the standard Wiener process dW can be collected from Eq. (3). Utilizing Eq. (1), an estimate of the system state can be obtained and utilized to construct a feedback controller.

In this paper, we consider the DRL-based feedback stabilization of the target quantum states. We will show our algorithm in stabilizing a GHZ entangled states of a three-qubit system and an eigenstate of an angular momentum system, while our scheme has the potential to be extended to other quantum systems.

III. DEEP REINFORCEMENT LEARNING

Abstracting a real-world problem into a Markov decision process (MDP) serves as the foundational step in applying DRL [29]. MDP provides a formal framework for modeling the interaction between an agent and its environment (quantum

systems in this work), offering a structured specification of the agent’s decision-making problem. The environment is abstracted with essential elements such as states, actions, rewards, and more, effectively describing the dynamic interaction between the agent and the external world. The agent is a pivotal component of DRL, representing a learning entity or decision-maker that, through interactions with the environment, learns to take actions to achieve objectives and continually refines its decision strategies to enhance the effectiveness of its actions. This process of agent-environment interaction and learning constitutes the core mechanism through which DRL efficiently tackles real-world challenges and achieves desirable outcomes.

An MDP is a structured representation denoted by the tuple $\langle \mathcal{S}, \mathcal{A}, R, P, \gamma \rangle$, where each element serves as a crucial role in modeling the problem and applying DRL:

- $\mathcal{S} = \{\rho \in \mathbb{H} : \rho = \rho^\dagger, \text{Tr}(\rho) = 1, \rho \geq 0\}$ represents the set of states. At each time step t , the environment presents a specific quantum state ρ_t to the agent, who subsequently makes decisions based on this state.
- \mathcal{A} signifies the set of actions, incorporating the actions $a_t \in \mathcal{A}$ that the agent can undertake at each time step. In this context, the actions correspond to the control signals $u_j(t)$ defined in Eq. (1), with values ranging from any bounded control strength, for example, $[0, 1]$ in this paper.
- R denotes the reward function, where the immediate reward r_t at time t can be influenced by the current state ρ_t , the action a_t , and the subsequent state ρ_{t+1} [25]:

$$r_t = R(\rho_t, a_t, \rho_{t+1}). \quad (4)$$

This paper considers the task of stabilizing the current state to the target state, thus the reward r_t can be simplified as

$$r_t = R(\rho_t). \quad (5)$$

At each time step, the agent receives an immediate reward based on the current state ρ_t . In this study, our reward function is associated with the trace-based distance D_{ρ_t} between the current state ρ_t and the target state ρ_d :

$$D_{\rho_t} \triangleq 1 - \text{Tr}(\rho_d \rho_t). \quad (6)$$

For common entangled states such as Bell states and GHZ states, when the distance $D_{\rho_t} = 0$, the system state is stabilized at the target state. The agent’s objective is to learn an optimal policy by maximizing the long-term cumulative reward.

- $P(\rho_{t+1}|\rho_t, a_t)$ is the state transition function. It indicates how the environment transitions to the next state ρ_{t+1} after taking action a_t in the current state ρ_t . It is consistent with the stochastic evolution of the quantum system described in Eq. (1), capturing the dynamic nature and randomness of the environment.
- γ is the discount factor, which strikes a balance between the significance of immediate rewards and future rewards. It determines the emphasis placed on future rewards, influencing the agent’s decision-making process in a long-term perspective.

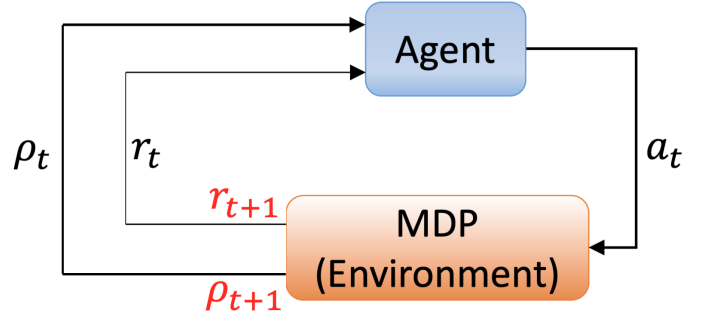


Fig. 1. Illustration of MDP for Agent-Environment interaction.

An MDP is a time-dependent and ongoing process, involving continuous interaction between the agent and the environment. The interaction can be illustrated as shown in Figure 1. For simplicity, we consider the interaction between the agent and the environment as a discrete time series (e.g., $t = 0, 1, 2, 3, \dots$). Starting from $t = 0$ with the known initial state ρ_0 , the agent selects an action a_0 based on the density matrix of ρ_0 and applies it to the environment. Subsequently, the environment undergoes a state transition according to the state transition function $P(\rho_{t+1}|\rho_t, a_t)$, resulting in the next state ρ_1 , and provides an immediate reward r_1 based on the reward function R . The environment also utilizes a classical computer to solve the SME (1) to estimate the density matrix of ρ_1 , which is then fed back to the agent. This process is iterated until completion. Therefore, the MDP and the agent jointly generate a sequence or trajectory as follows:

$$\rho_0, r_0, a_0, \rho_1, r_1, a_1, \rho_2, r_2, a_2, \rho_3, r_3, \dots$$

The function that selects an action a from the set of actions \mathcal{A} based on the current state ρ is referred to as a policy $\pi(a|\rho)$. It simulates a mapping function between state inputs and action outputs. The objective of the MDP is to find the policy $\pi(a|\rho)$ that allows the agent to make optimal decisions, effectively maximizing long-term cumulative rewards. It is important to note that the resulting state ρ may not be a valid quantum state due to the inherent randomness in measurements and cumulative errors in solving the SME equation using classical computers [30]. For example, the state matrix may contain non-physical (negative) eigenvalues. To address this issue, a suitable approach is to check the eigenvalues of the estimated matrix at each step. When negative values are encountered, the state should be projected back onto a valid physical state. This can be achieved by finding the closest density matrix under the 2-norm [31]. This approximation ensures that a non-physical density matrix is transformed into the most probable positive semi-definite quantum state with a trace equal to 1.

DRL has proven to be a highly effective approach for solving MDP problems by using deep neural networks to approximate the policy function $\pi(a|\rho)$ of the agent. This enables DRL to solve high-dimensional and complex decision-making problems efficiently. DRL can automatically extract meaningful features from raw inputs and undergo end-to-end training within the reinforcement learning framework [32].

Existing DRL methods can be categorized into three main

types: value-based methods, policy-based methods, and actor-critic methods. The value-based approach aims to learn an action-value function $Q(\rho, a)$ which represents the value of taking an action a in state ρ . The agent typically uses an ϵ -greedy approach to select the appropriate action in a given state, resulting in a policy function $\pi(a|\rho)$ that guides the agent's decision; there is no explicit policy in the learning process. One well-known algorithm in this category is DQN [16], which uses a deep neural network to approximate the value function and iteratively updates the network to approximate the optimal value function, allowing for optimal decision-making.

Policy-based methods directly learn the policy function $\pi(a|\rho)$, which represents the probability distribution of selecting action a given state ρ . This approach is advantageous for handling continuous action spaces. A common algorithm in this category is policy gradient (PG) [33], which maximizes cumulative rewards using gradient ascent to improve policy performance.

Actor-critic methods are a hybrid approach that simultaneously learns the value function and policy function. The policy function, known as the "actor", interacts with the environment by selecting actions based on the current state, while the value function, known as the "critic", evaluates the value of actions. This method leverages the experience of the actor to enhance the critic's evaluation and, in turn, improves the actor's policy through the critic's evaluation [34].

Overall, these three categories of DRL methods offer distinct approaches to address various challenges and provide a wide range of techniques for learning optimal decision-making policies. In the following section, we delve into the fundamental principles of the DRL, leading to the application of the highly effective actor-critic style proximal policy optimization (PPO) algorithm [35] in this paper.

IV. APPLYING DRL TO QUANTUM MEASUREMENT-BASED FEEDBACK CONTROL

In this section, we apply the DRL to the quantum systems and aim to design a measurement-based feedback strategy to stabilize a given target state. The application is comprised of training and testing parts. In the training part, the primary objective lies in the agent's policy function $\pi_\theta(a|\rho)$, constructed by a neural network with the adjustable parameter set θ . This parameter set is updated aiming for a higher reward by using data that is generated through the interaction between the agent and the environment. Once the agent finishes training, it can be applied to the quantum systems to generate real-time feedback control signals in achieving the stabilization of target states.

A. Environment: States and Actions

The two most basic elements of the environment are states and actions. The prior step in applying DRL is to convert the quantum states into a form that can be recognized by DRL. To facilitate agent training and testing, the quantum density matrix is sequentially flattened into a list that contains both the real and imaginary parts (vectorization). For example, the density matrix $\rho = \begin{bmatrix} \alpha_1 + \beta_1 i & \alpha_2 + \beta_2 i \\ \alpha_3 + \beta_3 i & \alpha_4 + \beta_4 i \end{bmatrix}$ of a single qubit

is transformed into $\rho := [\alpha_1, \alpha_2, \alpha_3, \alpha_4, \beta_1, \beta_2, \beta_3, \beta_4]^T$. Additionally, in order to better diagnose the learned policy, the current evolution time is also included as one of the observed states during agent training. By having access to the current time, the agent is more likely to exhibit improved performance [36]. Therefore, the observation received by the agent is in the form of $\rho(t) := [\alpha_1, \alpha_2, \alpha_3, \alpha_4, \beta_1, \beta_2, \beta_3, \beta_4, t]^T$.

As for actions, the policy specifies the control signals corresponding to control Hamiltonians. For example, if the system in Eq. (1) has two control Hamiltonians H_1 and H_2 , the actions for each time step are in the form of $a := [u_1, u_2]^T$.

Guided by the policy $\pi_\theta(a|\rho)$, the agent stochastically selects an action a_t for an environmental state ρ_t . The environment then transitions to a new state ρ_{t+1} and provides an immediate reward r_t . Subsequently, the agent selects a new action a_{t+1} based on the updated state ρ_{t+1} , and this cycle continues until a predefined termination criterion is met, such as reaching a maximum step count, achieving a goal, or exceeding an acceptable error threshold. This iterative process is termed an episode (or sequence) $\tau = \{\rho_0, a_0, \rho_1, a_1, \dots, \rho_m\}$, where m denotes the final step of the episode, and $\tau \in \mathbb{D} = \{\tau_n\}_{n=1,2,\dots,N}$, with N denoting the total number of possible sequences. Without any confusion, we use τ in the following to represent one episode. The agent's primary objective is to maximize a measure of expected cumulative reward across all potential episodes.

B. Reward

The immediate reward r_t at each step is closely related to the distance D_{ρ_t} in Eq. (6). We expect a positive reward as the distance approaches 0. To encourage the system to reach the target state, inspired by the inverse proportional functional form, we define a reward function (IPF Reward) with different behaviors based on the distance to the goal state as

$$r_t = \left(\frac{\bar{D} - \underline{D}}{\mathfrak{f} * (D_{\rho_t} - \underline{D}) - \mathfrak{e} * (D_{\rho_t} - \bar{D})} - \frac{1}{\mathfrak{f}} \right) \times \left(\frac{\mathfrak{e}\mathfrak{f} * (\bar{R} - \underline{R})}{\mathfrak{f} - \mathfrak{e}} \right) + \underline{R}, \quad (7)$$

where \bar{D} and \underline{D} as the upper and lower bounds of the distance D_{ρ_t} , respectively, and \bar{R} and \underline{R} as the upper and lower bounds of the reward, respectively. In this way, we can set the numerical values of these four bounds to assign different rewards to different D_{ρ_t} . Additionally, we use \mathfrak{e} and \mathfrak{f} to regulate the slope of the reward curve. In this paper, we set $\mathfrak{e} = 2$ and $\mathfrak{f} = 10$. The different slopes imply that different distances have different importance for the DRL agent.

When the distance $D_{\rho_t} \leq 0.001$, the state is considered nearly ready for success, and the system deserves a positive reward. As shown in Figure 2(a), when the distance is between 0.001 and 0 (i.e., $\bar{D} = 0.001$ and $\underline{D} = 0$), we set the reward boundaries to range from 1 to 100 (i.e., $\bar{R} = 100$ and $\underline{R} = 1$). The closer the distance is to 0, the larger the positive reward is given. The steepening slope of the reward curve as the system approaches the goal underscores the urgency of achieving the target state rapidly. This design enforces the agent's commitment to swift and accurate goal attainment.

However, providing positive rewards only when the target is achieved can lead to the reward sparse problem in reinforcement learning [37]. In the absence of supplementary guidance to direct the agent towards the correct trajectory prior to engaging with the objective, the agent is likely to encounter substantial difficulties in accomplishing the mission solely through random exploration. To address this issue, we introduce a negative reward (penalty) at each step when the system is not in the vicinity of the target state. The punishment range is set to $[-0.1, 0]$ as depicted in Figure 2(b). When $D_{\rho_t} = 1$, a punishment of -0.1 is given. As the distance D_{ρ_t} decreases, indicating that the system state is getting closer to the goal, the punishment decreases faster (represented by a steeper slope). When the distance reaches 0.001, the previously described positive reward in Figure 2(a) takes over.

Remark 1: When the distance D_{ρ_t} approaches 0.001, we choose to gradually reduce the penalties rather than increase positive rewards. This decision is made to stabilize the DRL agent during training and mitigate the issues related to reward hacking [38]. For instance, if we were to provide progressively larger rewards as D approaches 0.001, the agent might be inclined to persist near 0.001 until reaching the maximum number of steps in the episode, as this would yield simpler and higher cumulative rewards. By applying small penalties at each step, we encourage the agent to explore the state space more extensively. Our aim is to prevent the agent from becoming overly fixated on known high-reward regions while neglecting other unknown regions that may offer higher rewards. Instead, we prompt the agent to reach the goal promptly and iteratively improve its policy to enhance performance.

Additionally, recognizing the desirability of swiftly stabilizing the system to the target state, we introduce a small additional penalty associated with the current number of evolutionary steps. Prior to system stabilization at the target, an additional penalty proportional to the number of steps is applied. For instance, the first step incurs a penalty of -1×10^{-6} , the second step incurs -2×10^{-6} , and so forth.

In summation, the outlined approach encompasses the design of instantaneous rewards for each step. This reward design encourages the agent to explore and discover more possibilities while guiding it to reach the target state quickly, and effectively. The balance between positive rewards when close to the goal and negative rewards when away from it helps the agent to learn from both “good” and “bad” actions, leading to a more robust and effective learning process. We show the superiority of our design by simulating different reward functions in the Appendix.

With this reward function, we are now in the position to maximize the cumulative expected reward of the sequence, so for a complete sequences τ , its cumulative reward can be expressed as

$$R(\tau) = \sum_{t=0}^m A^\theta(\rho_t, a_t). \quad (8)$$

$A^\theta(\rho_t, a_t) = Q(\rho_t, a_t) - V^\phi(\rho_t)$ is known as the advantage function in the field of reinforcement learning, which is utilized to assess the desirability of taking a specific action a_t at state ρ_t . $Q(\rho_t, a_t) = \sum_{t'=t}^m \gamma^{t'-t} r_{t'}$ represents the action-

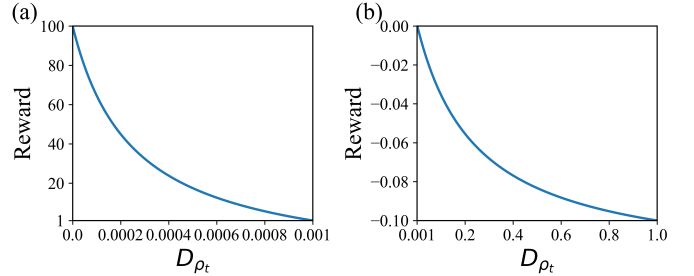


Fig. 2. Reward Function. (a) When the D_{ρ_t} is between 0.001 and 0, we consider that the current system is almost approaching the target state. A smaller D_{ρ_t} value corresponds to a larger positive reward. When $D_{\rho_t} = 0$, the maximum reward $r = 100$ is obtained. (b) When the D_{ρ_t} is between 1 and 0.001, we consider that there is still distance between the current state and the target state. At $D_{\rho_t} = 1$, the maximum negative reward (penalty) is imposed, and as the D_{ρ_t} value decreases, the penalty decreases accordingly.

value function, indicating the expected discounted reward for choosing action a_t in state ρ_t , i.e., the cumulative sum of rewards until the end of the episode after executing this action. $r_{t'}$ is the reward function in Eq. (7). The value of γ lies between 0 and 1, determining the emphasis on long-term rewards (close to 1) or short-term rewards (close to 0). It effectively introduces a discounting mechanism for future rewards, thereby shaping the agent’s preference for future reward consideration when making decisions. $V^\phi(\rho_t)$ is referred to as the state-value function (or baseline) and is modeled by a neural network with the same structure as the policy network but with different parameters ϕ . It is primarily employed to approximate the discounted rewards from state ρ_t to the end of an episode. Specifically, if the current state is ρ_t , and for all possible actions $a_t^{(1)}, a_t^{(2)}, \dots, a_t^{(\dots)}$, they correspond to discounted rewards $Q(\rho_t, a_t^{(1)}), Q(\rho_t, a_t^{(2)}), \dots, Q(\rho_t, a_t^{(\dots)})$. As $V^\phi(\rho_t)$ represents the expected value of the discounted rewards at ρ_t , we can use $Q(\rho_t, a_t^{(1)}), Q(\rho_t, a_t^{(2)}), \dots, Q(\rho_t, a_t^{(\dots)})$ as features to approximate the value of $V^\phi(\rho_t)$, representing the expected value of rewards in state ρ_t . When $A^\theta(\rho_t, a_t) > 0$, action a_t is considered better than average and is worth increasing the probability of being chosen in subsequent iterations while decreasing the probability otherwise.

C. Core Algorithmic Ideas for DRL Agents

The probability of each sequence occurring is multiplied by its corresponding cumulative reward, and the sum of these products yields the expected reward. The probability of a specific τ sequence occurring given θ is defined as:

$$p_\theta(\tau) = \prod_{t=0}^m p_\theta(a_t | \rho_t) p(\rho_{t+1} | \rho_t, a_t). \quad (9)$$

We denote $p(\text{EVENT})$ to signify the probability of the occurrence of the EVENT. For example, $p_\theta(a_t | \rho_t)$ represents the probability of agent to choose action a_t given ρ_t while $p(\rho_{t+1} | \rho_t, a_t)$ represents the probability of environment transiting at ρ_{t+1} from ρ_t given the action a_t applied.

When the parameter θ is given, the expected value of the total reward, denoted as $J(\theta)$, is evaluated as the weighted

sum of each sampled τ sequence, expressed by

$$J(\theta) = \sum_{\tau} R(\tau) p_{\theta}(\tau) := \mathbb{E}_{\tau \sim p_{\theta}(\tau)} [R(\tau)]. \quad (10)$$

To maximize $J(\theta)$, which indicates that our chosen policy parameters θ can lead to higher average rewards, we adopt the well-known gradient descent method. Thus, we take the derivative of the expected reward $J(\theta)$ in Eq. (10), resulting in the expression shown in

$$\begin{aligned} \nabla J(\theta) &= \sum_{\tau} R(\tau) \nabla p_{\theta}(\tau) \\ &= \sum_{\tau} R(\tau) p_{\theta}(\tau) \nabla \log p_{\theta}(\tau) \\ &= \sum_{\tau} R(\tau) p_{\theta}(\tau) \sum_{t=0}^m \nabla \log p_{\theta}(a_t | \rho_t) \\ &= \mathbb{E}_{\tau \sim p_{\theta}(\tau)} \left[R(\tau) \sum_{t=0}^m \nabla \log p_{\theta}(a_t | \rho_t) \right] \\ &\approx \mathbb{E}_{(\rho_t, a_t) \sim \pi_{\theta}} \left[\nabla \log p_{\theta}(a_t | \rho_t) A^{\theta}(\rho_t, a_t) \right]. \end{aligned} \quad (11)$$

We use $\nabla f(x) = f(x) \nabla \log f(x)$ to derive the second row of Eq. (11). The last approximate equation is a result of practical gradient computations, where instead of calculating the expected reward for an entire trajectory, rewards contributed by each individual state-action pair (ρ, a) are computed separately. These individual rewards are then summed up to obtain the total cumulative reward for the optimization process. The direction of the policy update $\pi_{\theta}(a|\rho)$ is biased towards favoring state-action pairs that contribute to higher cumulative rewards within the sequence. For instance, if an action a executed in state ρ leads to a positive cumulative discounted reward, the subsequent update will enhance the probability of choosing action a in state ρ , while diminishing the likelihood of selecting other actions. The update equation for the parameters θ is as follows:

$$\theta = \theta + \eta \nabla J(\theta), \quad (12)$$

where η is the learning rate.

Once the policy $\pi_{\theta}(a|\rho)$ is updated, it necessitates the reacquisition of training data prior to the subsequent policy update. This arises due to the alteration in the probability distribution $p_{\theta}(\tau)$ brought about by the modified policy. Following data sampling, the parameter θ undergoes refinement, leading to the discarding of all prior data. Subsequent parameter updates mandate the collection of fresh data, constituting the fundamental principle underlying the conventional PG algorithm. However, in the context of quantum systems, the process of sampling system information is often characterized by time-intensive and computationally demanding operations. For instance, after each measurement, a classical computer is requisitioned to solve the SME (1) to ascertain the system's state in the subsequent moment. This inability to reuse previously acquired data contributes to a protracted training process. To address this challenge, an additional strategy $\pi_{\theta'}$ is introduced, mirroring the architecture of $\pi_{\theta}(a|\rho)$. Instead of directly engaging with the environment for data gathering, the

primary agent π_{θ} employs the auxiliary agent $\pi_{\theta'}$ to interact with the environment and accumulate data. The objective is to subsequently utilize this data to train π_{θ} multiple times, effectively reducing the computational and resource demands for data collection. Ensuring the consistency of data sampled by $\pi_{\theta'}$ with that of π_{θ} , importance sampling [39] is introduced to facilitate this synchronization process. This approach contributes to enhancing data reuse and the overall efficiency of the training procedure. Eq. (11) is updated as:

$$\begin{aligned} \nabla J(\theta) &= \mathbb{E}_{(\rho_t, a_t) \sim \pi_{\theta'}} \left[\frac{p_{\theta}(\rho_t, a_t)}{p_{\theta'}(\rho_t, a_t)} \nabla \log p_{\theta}(a_t | \rho_t) A^{\theta'}(\rho_t, a_t) \right] \\ &= \mathbb{E}_{(\rho_t, a_t) \sim \pi_{\theta'}} \left[\frac{p_{\theta}(a_t | \rho_t) p_{\theta}(\rho_t)}{p_{\theta'}(a_t | \rho_t) p_{\theta'}(\rho_t)} \nabla \log p_{\theta}(a_t | \rho_t) A^{\theta'}(\rho_t, a_t) \right] \\ &= \mathbb{E}_{(\rho_t, a_t) \sim \pi_{\theta'}} \left[\frac{p_{\theta}(a_t | \rho_t)}{p_{\theta'}(a_t | \rho_t)} \nabla \log p_{\theta}(a_t | \rho_t) A^{\theta'}(\rho_t, a_t) \right]. \end{aligned} \quad (13)$$

Here, all the state-action pairs (ρ_t, a_t) (or alternatively, all trajectories $\tau \in \mathbb{D}$) are sampled from $\pi_{\theta'}$, where $p_{\theta}(\rho_t, a_t)/p_{\theta'}(\rho_t, a_t)$ is the importance weight, dynamically adjusting the weight of the data sampled by $\pi_{\theta'}$ in real-time to more accurately estimate the expected value under the target policy π_{θ} .

The corresponding objective function from Eq. (13) can be calculated as:

$$J^{\theta'}(\theta) = \mathbb{E}_{(\rho_t, a_t) \sim \pi_{\theta'}} \left[\frac{p_{\theta}(a_t | \rho_t)}{p_{\theta'}(a_t | \rho_t)} A^{\theta'}(\rho_t, a_t) \right]. \quad (14)$$

Nonetheless, in the absence of constraint, such as when $A^{\theta'}(\rho_t, a_t) > 0$, indicating the desirability of specific action-state combinations, the agent's inclination would be to elevate their likelihood, effectively amplifying the $p_{\theta}(a_t | \rho_t)/p_{\theta'}(a_t | \rho_t)$ value. This scenario can lead to policy learning inaccuracies and an erratic learning process, impeding convergence. To counteract this, the PPO introduces a pivotal mechanism, termed the "clip ratio". This clip ratio imposition serves to confine the proportions between the new and preceding policies, thereby ensuring congruence and augmenting the algorithm's dependability. The following equation demonstrates the PPO Clipping algorithm, incorporating the clipping term to bound the difference between p_{θ} and $p_{\theta'}$ during the policy update.

$$\begin{aligned} J_{\text{PPO}}^{\theta'}(\theta) &\approx \mathbb{E}_{(\rho_t, a_t) \sim \pi_{\theta'}} \min \left(\varrho A^{\theta'}(\rho_t, a_t), \right. \\ &\quad \left. \text{clip} \left(\varrho, 1 - \varsigma, 1 + \varsigma \right) A^{\theta'}(\rho_t, a_t) \right), \end{aligned} \quad (15)$$

where $\varrho = p_{\theta}(a_t | \rho_t)/p_{\theta'}(a_t | \rho_t)$. The last two terms $1 - \varsigma$, and $1 + \varsigma$ in the clip function limit the boundaries of the first term. ς is a hyperparameter, typically set to 0.1 or 0.2. Exhaustively considering all possible sequences is typically infeasible, and thus in practical training, the objective function (15) is often

formulated in the following manner:

$$J_{\text{PPO}}^{\theta'}(\theta) \approx \frac{1}{Nm} \sum_{\tau \in \mathbb{D}} \sum_{t=0}^m \min \left(\varrho A^{\theta'}(\rho_t, a_t), \text{clip} \left(\varrho, 1 - \varsigma, 1 + \varsigma \right) A^{\theta'}(\rho_t, a_t) \right), \quad (16)$$

where N and m represent finite real numbers that respectively signify the count of collected sequences and the maximum number of steps within each sequence.

Based on the above, we can see that PPO has three sets of network parameters for its update strategy:

- One set of main policy parameters θ , which is updated every time.
- One set of policy parameter copies θ' , which interact with the environment and collect data. They utilize importance sampling to assist in updating the main policy parameters θ . Typically, θ' is updated only after several updates of θ has been performed.
- One set of value network parameters ϕ , which are updated based on the collected data using supervised learning to update the evaluation of states. They are also updated every time.

D. Training

Our DRL algorithm is implemented using the open-source Python library Stable-Baselines3 [40], while the quantum dynamic environment is constructed within the Gymnasium framework [41]. All simulations in this study are conducted on a computer equipped with an Apple M1 Pro chip and 32 GB of memory, utilizing Python 3.11.3, stable-baselines3 2.3.2, and Gymnasium 0.29.1. We design a reasonable reward function to guide the DRL agent through iterative learning, aiming to train an excellent DRL agent capable of generating control signals to achieve the stability of the target entangled state.

Initial State: During training, the state is randomly reset to a quantum state after the completion of each episode, which means that at each episode in the training iteration, the agent starts from a new state and explores the environment from that point.

Neural Network Architecture: Each policy π_{θ} is represented by a neural network that maps a given state ρ to a probability distribution over actions a . The action distribution is modeled as a gaussian distribution. The input layer is processed by two fully connected hidden layers, each with 128 neurons, accompanied by a linear output layer with the same dimension as the action space (2 in this paper). All hidden layers use the Tanh activation function. The value function $V^{\phi}(\rho_t)$ is composed of a similar neural network architecture, with the only difference being that the output layer is a single linear unit used to estimate the state-value function. The value function $V^{\phi}(\rho_t)$ is estimated using the temporal difference (TD) method [42]. Then, the generalized advantage estimator (GAE) [43] is employed to compute the advantage function in Eq. (8), which is subsequently used in Eq. (15) to calculate the gradient for updating the policy π_{θ} .

Learning Rate: The learning rate is a hyperparameter that determines the step size of the algorithm's updates based on observed rewards and experiences during training. In our training process, the learning rate η is not a constant value but follows a linear schedule. Our learning rate starts at $\eta = 5 * 10^{-7}$ and linearly decreases over time during the training process. This allows the algorithm to explore more in the early stages of training when the policy might be far from optimal. As the training progresses, the policy approaches convergence, and the learning rate decreases to promote stability in the learning process and fine-tune the policy around the optimal solution. This helps the DRL agent achieve better performance and stability during the training process. Please refer to [42], [44] for more details.

Early Termination: Regarding early termination, continuous quantum measurement feedback control can be modeled as an infinite-horizon MDP, but during training, each episode is simulated on a finite time horizon. Additionally, practical applications require a finite system evolution time. Therefore, we set fixed duration or termination conditions to end an episode. The termination conditions include the following:

- When the distance $D_{\rho_t} \in [0, 0.001]$ for 10 consecutive measurements, multiple measurements verifying that the system is in the target state are considered mission complete.
- In a specific system, the maximum training time for a trajectory is set to a fixed value. For example, for the two-qubit state stabilization problem in section V-A, we set the maximum training time $T = 20$ arbitrary units (a.u.). When the evolution time reaches 20 a.u., regardless of whether it has converged to the goal or not, the training trajectory is halted. This approach not only greatly saves training time but also significantly reduces the issue of overfitting.

These early termination conditions bias the data distribution towards samples that are more relevant to the task, thereby saving training time and preventing undesirable behaviors. During agent testing, the time is typically not limited to evaluate the agent's performance in a real environment and assess its ability to complete tasks within a reasonable time frame.

The pseudo-code for the PPO in quantum state stabilization is shown in Algorithm 1.

V. NUMERICAL SIMULATION

A. Two-Qubit System

We first consider a system of two qubits in a symmetric dispersive interaction with an optical probe as proposed in [45]. We consider using the DRL control scheme mentioned above to address the two-qubit entangled state preparation problem for arbitrary initial quantum states. Denote the Pauli matrices

$$\sigma_x = \begin{bmatrix} 0 & 1 \\ 1 & 0 \end{bmatrix}, \quad \sigma_y = \begin{bmatrix} 0 & -i \\ i & 0 \end{bmatrix}, \quad \sigma_z = \begin{bmatrix} 1 & 0 \\ 0 & -1 \end{bmatrix}.$$

Algorithm 1 PPO for Quantum Feedback Control

Begin
Initial policy weights θ
Initial value function weights ϕ
repeat
 Sampling training data from the environment
 for $t = 0, 1, \dots$ **do**
 $\rho_t \leftarrow$ start state
 $r_t \leftarrow$ reward
 $a_t \sim \pi_\theta(a_t | \rho_t)$
 Apply a and simulate the system one step forward
 $\rho_{t+1} \leftarrow$ end state
 $r_{t+1} \leftarrow$ reward
 Record $(\rho_t, r_t, a_t, \rho_{t+1})$ into memory M
 end for
 $\theta' \leftarrow \theta$
for each update **do**
 Sample Nm samples $\{(\rho_t, r_t, a_t, \rho_{t+1})\}$ from M
 Update main policy:
 for each $(\rho_t, r_t, a_t, \rho_{t+1})$ **do**
 compute advantage A^θ in Eq. (8) using current V^ϕ
 and GAE
 compute $\frac{p_\theta(a_t | \rho_t)}{p_{\theta'}(a_t | \rho_t)}$
 end for
 Calculate the gradient to update the policy parameters
 θ via Eq. (16)
 Update value function V^ϕ :
 for each $(\rho_t, r_t, a_t, \rho_{t+1})$ **do**
 Use TD to update the value function V^ϕ
 end for
end for
until The training termination condition is triggered

Control Hamiltonians H_1 and H_2 are

$$H_1 = \sigma_y \otimes I_2 = \begin{bmatrix} 0 & 0 & -i & 0 \\ 0 & 0 & 0 & -i \\ i & 0 & 0 & 0 \\ 0 & i & 0 & 0 \end{bmatrix},$$

$$H_2 = I_2 \otimes \sigma_y = \begin{bmatrix} 0 & -i & 0 & 0 \\ i & 0 & 0 & 0 \\ 0 & 0 & 0 & -i \\ 0 & 0 & i & 0 \end{bmatrix},$$

respectively. Angular momentum operator

$$c = \sigma_z \otimes I_2 + I_2 \otimes \sigma_z = \begin{bmatrix} 2 & 0 & 0 & 0 \\ 0 & 0 & 0 & 0 \\ 0 & 0 & 0 & 0 \\ 0 & 0 & 0 & -2 \end{bmatrix}.$$

Specify the target state as

$$\rho_d = \begin{bmatrix} 0 & 0 & 0 & 0 \\ 0 & 0.5 & 0.5 & 0 \\ 0 & 0.5 & 0.5 & 0 \\ 0 & 0 & 0 & 0 \end{bmatrix},$$

which is a symmetric two-qubit state.

We utilize the previously summarized PPO algorithm to train the DRL agent. For the training trajectories, we set a time interval of $\Delta t = 0.001$ a.u. for each measurement step, with a maximum evolution time of $T = 20$ a.u., corresponding to a maximum of 20,000 steps. At each step, the DRL agent interacts with the environment, obtaining system information to generate control signals, which are then stored for iterative updates of the policy. The total number of training steps is set to 10^7 . On our computer, training takes approximately 50 minutes. However, as our primary focus is on the performance of the trained agent, the training duration is not of critical importance. In practical experiments, it is feasible to pre-train the agent; once trained, the agent can be directly utilized.

In order to evaluate its performance, we test the proposed strategy on 50 randomly selected distinct initial quantum states ρ_0 (corresponding to different initial distances D_{ρ_0} , as indicated by the blue line in Figure 3). The light blue lines represent the evolution trajectory of a specific initial state with respect to the target state, averaged over 50 different trajectories under varying environmental noise, while the dark blue line depicts the average evolutionary trajectory of all the different initial states. A distance of $D_{\rho_t} = 0$ indicates the system stabilizing at the target state. It is worth noting that the well-trained agent successfully stabilizes any initial state to the target state. Furthermore, for comparison with the Lyapunov method mentioned in [45], we retain the same 50 sets of randomly selected initial states and obtain the orange trajectories in Figure 3 using the Lyapunov method. It can be observed that the control signals generated by the DRL agent outperform the Lyapunov method. Assuming we take the time when the distance D_{ρ_t} becomes less than 0.001 as the required evolution time of the system, under the guidance of the DRL agent, the average evolution time is 5.64 a.u., while the average time using the Lyapunov method is 14.36 a.u.. The DRL's average stabilization time is improved by 60.72% over the Lyapunov method. This indicates that our DRL approach successfully stabilizes these quantum states to the target state faster than the Lyapunov method.

B. GHZ State

We then consider a more complex problem of preparing three-qubit entangled GHZ states, which are special entangled states and have been regarded as maximally entangled states in many measures [46], [47]. A GHZ entangled state is defined in the following form [46], [48]:

$$|\text{GHZ}\rangle = \frac{1}{\sqrt{2}}(|0\rangle^{\otimes n} + |1\rangle^{\otimes n}), \quad (17)$$

where n is the number of qubits. Its density matrix can be expressed as $\rho_{\text{GHZ}} \triangleq |\text{GHZ}\rangle\langle\text{GHZ}|$. For the three-qubit GHZ state, we choose $|\text{GHZ}\rangle = (1/\sqrt{2})(|000\rangle + |111\rangle)$, which gives

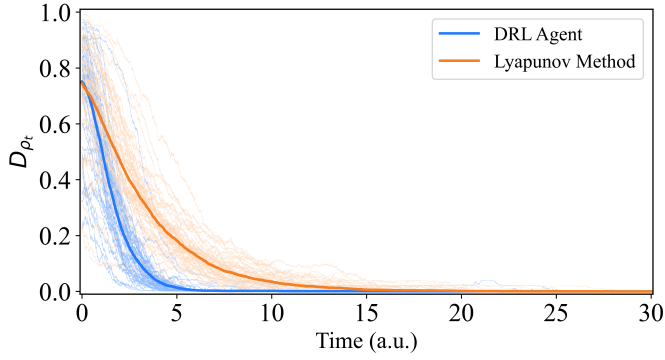


Fig. 3. Evolution of the distance D_{ρ_t} for 50 random initial states stabilized to the target Two-Qubit state under the control of the DRL agent (blue) and Lyapunov method (orange). The average stabilization time to the target under DRL control is 5.64 a.u., while the Lyapunov method requires an average time of 14.36 a.u.. (The stabilization time is defined as the time when the distance $D_{\rho_t} \leq 0.001$.) The light blue (orange) lines represent the average evolution trajectories for different initial states, and the dark blue (orange) line represents the average trajectory across all different initial states.

the following density matrix:

$$\rho_{\text{GHZ}} = \frac{1}{2} \begin{bmatrix} 1 & 0 & 0 & 0 & 0 & 0 & 0 & 0 & 1 \\ 0 & 0 & 0 & 0 & 0 & 0 & 0 & 0 & 0 \\ 0 & 0 & 0 & 0 & 0 & 0 & 0 & 0 & 0 \\ 0 & 0 & 0 & 0 & 0 & 0 & 0 & 0 & 0 \\ 0 & 0 & 0 & 0 & 0 & 0 & 0 & 0 & 0 \\ 0 & 0 & 0 & 0 & 0 & 0 & 0 & 0 & 0 \\ 0 & 0 & 0 & 0 & 0 & 0 & 0 & 0 & 0 \\ 1 & 0 & 0 & 0 & 0 & 0 & 0 & 0 & 1 \end{bmatrix}. \quad (18)$$

A degenerate observable c is required according to the quantum state collapse after measurement [8], [45], [49]. The quantum state collapse states that the system in Eq. (1) will randomly converge to an eigenstate or eigenspace of c without any control. Hence, we choose an observable in the following diagonal form:

$$c = \text{diag}[\lambda_d, \lambda_2, \dots, \lambda_{n-1}, \lambda_d], \quad (19)$$

where $\lambda_d \neq \lambda_k$ ($k = 2, \dots, n-1$), and λ_d is the eigenvalue corresponding to the target state ρ_d , i.e., $c\rho_d = \lambda_d\rho_d$.

Due to the degenerate form of the observable c in Eq. (19), the system may converge to other state in the corresponding eigenspace related to λ_d , two control channels u_1 and u_2 based on Lyapunov method have been applied in [8], [45], [49] to solve this problem. For subsequent performance comparisons, two control channels are also used in this paper.

For any training trajectory, we take a time interval $\Delta t = 0.001$ a.u. for each measurement step. Given that we have set the maximum evolution time as $T = 40$ a.u., it means the maximum number of evolution steps for any trajectory during training is 40,000. The total number of training steps is 10^8 .

For all instances, in order to compare with the Lyapunov methods presented in [8], we choose the same system Hamiltonian as $H_0 = \text{diag}[1, -1, -1, 1, 1, -1, -1, 1]$, the target state as $\rho_d \triangleq \rho_{\text{GHZ}}$ (18), and the observable c as

$$\begin{aligned} c &= 2 \times (\sigma_z \otimes \sigma_z \otimes I_2) + I_2 \otimes \sigma_z \otimes \sigma_z \\ &= \text{diag}[3, 1, -3, -1, -1, -3, 1, 3]. \end{aligned} \quad (20)$$

The control Hamiltonians H_1 and H_2 are chosen as

$$\begin{aligned} H_1 &= I_2 \otimes I_2 \otimes \sigma_x + \sigma_x \otimes \sigma_x \otimes I_2 \quad (21) \\ &= \begin{bmatrix} 0 & 1 & 0 & 0 & 0 & 0 & -1 & 0 \\ 1 & 0 & 0 & 0 & 0 & 0 & 0 & -1 \\ 0 & 0 & 0 & 1 & -1 & 0 & 0 & 0 \\ 0 & 0 & 1 & 0 & 0 & -1 & 0 & 0 \\ 0 & 0 & -1 & 0 & 0 & 1 & 0 & 0 \\ 0 & 0 & 0 & -1 & 1 & 0 & 0 & 0 \\ -1 & 0 & 0 & 0 & 0 & 0 & 0 & 1 \\ 0 & -1 & 0 & 0 & 0 & 0 & 1 & 0 \end{bmatrix}, \end{aligned}$$

and

$$\begin{aligned} H_2 &= \sigma_x \otimes I_2 \otimes I_2 + I_2 \otimes \sigma_x \otimes \sigma_x \quad (22) \\ &= \begin{bmatrix} 1 & 0 & 0 & 1 & 0 & 0 & 0 & 0 \\ 0 & 1 & 1 & 0 & 0 & 0 & 0 & 0 \\ 0 & 1 & 1 & 0 & 0 & 0 & 0 & 0 \\ 1 & 0 & 0 & 1 & 0 & 0 & 0 & 0 \\ 0 & 0 & 0 & 0 & -1 & 0 & 0 & 1 \\ 0 & 0 & 0 & 0 & 0 & -1 & 1 & 0 \\ 0 & 0 & 0 & 0 & 0 & 1 & -1 & 0 \\ 0 & 0 & 0 & 0 & 1 & 0 & 0 & -1 \end{bmatrix}. \end{aligned}$$

We test the trained DRL agent in various environments to evaluate its performance and robustness. The goal is to assess how well the agent generalizes its learned policies to different scenarios and how it copes with perturbations and variations in the environment. To achieve this, we expose the trained DRL agent to a set of diverse environments, each with unique characteristics and challenges. These environments are carefully designed to represent a wide range of scenarios and potential disturbances that the agent might encounter in real-world applications. During the testing phase, we measure the agent's performance in terms of its ability to achieve the desired objectives and maintain stability in each environment. We also examine its response to changes in the measurement efficiency η_c and time delay disturbances to assess its robustness and adaptability.

We first investigate the ‘‘perfect case’’. In this paper, the ‘‘perfect case’’ entails assuming that negligible delay in solving the SME (1) by classical computers, and perfect detection, that is, measurement efficiency $\eta_c = 1$. In contrast, situations where there is delay or imperfect detection within the system are collectively referred to as ‘‘imperfect cases’’. We then show some performance indications for ‘‘imperfect cases’’.

1) *Stabilization of the GHZ state under perfect case:* We initiate the testing phase to evaluate the ability of arbitrary initial states to stabilize to the target GHZ state within a specified time frame. As shown in Figure 4, we employ the comparative approach mentioned in Section V-A, randomly selecting 50 distinct initial states for control using the DRL agent and the Lyapunov method. The blue and orange lines correspond to the DRL method and the Lyapunov method, respectively. Under the guidance of the DRL agent, the control strategy improved the average evolution time by 22.38% compared to the Lyapunov method (DRL: 33.39 a.u. vs. Lyapunov: 43.02 a.u.). This indicates that our DRL approach successfully stabilizes quantum states to the target GHZ state more rapidly.

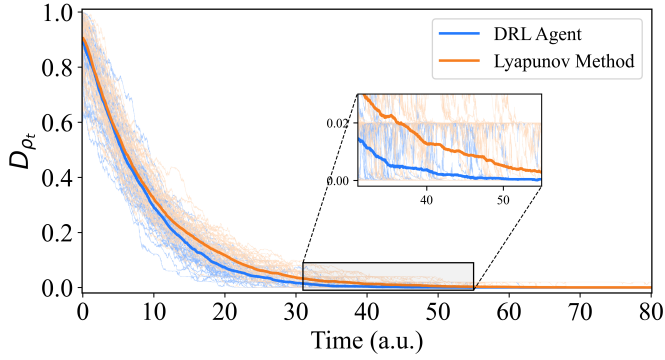


Fig. 4. Evolution of the distance D_{ρ_t} for 50 random initial states stabilized to the target GHZ state under the control of the DRL agent (blue) and Lyapunov method (orange). The average stabilization time to the target under DRL control is 33.39 a.u., while the Lyapunov method requires an average time of 43.02 a.u.. (The stabilization time is defined as the time when the distance $D_{\rho_t} \leq 0.001$.) The light blue (orange) lines represent the average evolution trajectories for different initial states, and the dark blue (orange) line represents the average trajectory across all different initial states.

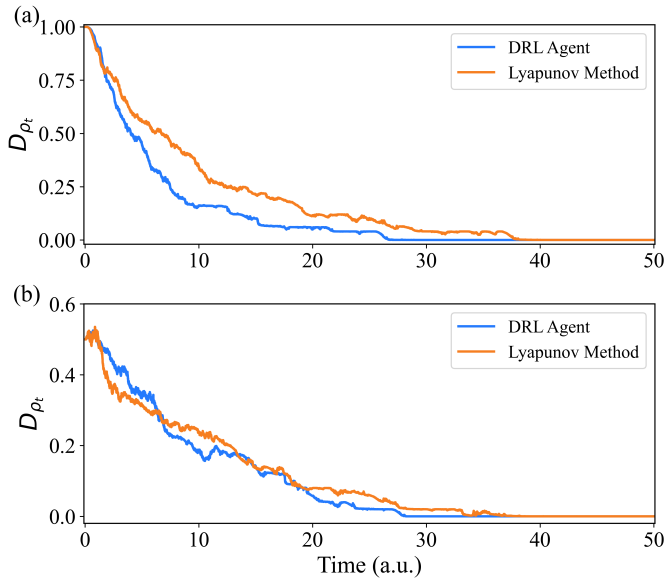


Fig. 5. Evolution of the distance D_{ρ_t} to stabilize two particular initial states (a) $\rho_0^1 = \text{diag}[0, 1, 0, 0, 0, 0, 0]$, (b) $\rho_0^2 = \text{diag}[1, 0, 0, 0, 0, 0, 0]$ to the target GHZ state under the control of the DRL agent (blue) and the Lyapunov method (orange). Each trajectory represents the average of 50 different stabilization processes for these specific initial states.

In addition, we also explore the evolution of two specific initial states, denoted as $\rho_0^1 = \text{diag}[0, 1, 0, 0, 0, 0, 0]$ and $\rho_0^2 = \text{diag}[1, 0, 0, 0, 0, 0, 0]$, mentioned in [8] as examples. We repeat their stabilization 50 times each to obtain averaged convergence curves that approximate the system's evolution. Figure 5(a) and Figure 5(b) depict the evolution of these two distinct initial states. The blue curve represents the evolution controlled by the DRL agent, while the orange curve represents the evolution controlled by the Lyapunov method from [8]. It can be observed that the well-trained DRL agent not only achieves stable convergence to the target state but also showcases faster convergence compared to the Lyapunov method.

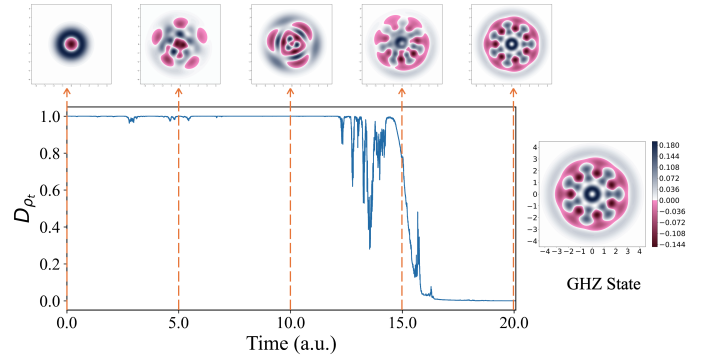


Fig. 6. One specific (not averaged) evolutionary trajectory of the distance D_{ρ_t} under the control of the DRL agent, starting from the initial state ρ_0^1 . The top five images depict the Wigner function for a harmonic mode of the system at different moments during the evolution. The figure on the right shows the phase-space probability distributions of the standard three-qubit GHZ state, which serves as a reference.

We randomly select a single trajectory under the control of a DRL agent with initial state ρ_0^1 . The left subplot of Figure 6 illustrates the evolutionary trajectory with D_{ρ_t} , and the top images display the Wigner function for a harmonic mode of the system state at five different evolution times. In contrast, the subplot on the right serves as a reference plot for the target three-qubit GHZ state. A comparison reveals that the phase-space distribution of the system state gradually approaches the target state over time, and at $t = 20$ a.u., the system state is identical to the target state.

In practical agent training and application, uncertainties often exist. For example, the efficiency of measurements is typically not perfect, and there are frequently issues related to time delays in the feedback process. In the following two subsections we explore the robustness of our DRL agent to these two imperfections.

2) *Stabilization of the GHZ state with imperfect measurement:* We start from the measurement inefficiency. It's important to note that we are using the agent trained under the assumption of “perfect case” to test the robustness of the agent. We assume a measurement efficiency $\eta_c = 0.8$, which represents a relatively high efficiency achievable in current laboratory settings [50]. As shown in the Figure 7, 50 randomly selected initial states are successfully stabilized to the target GHZ state under the control of the agent. Therefore, our trained DRL agent has shown good robustness in terms of measurement inefficiency.

3) *Stabilization of the GHZ state with time delay:* We then consider the issue of time delay in feedback processes. Especially in the rapid evolution of quantum systems, the time required for traditional computers to solve the SME (1) is often non-negligible. Therefore, it is worth considering incorporating a fixed compensation for time during the testing process of the agent. For instance, assuming a time delay of $\sqcup = 0.05$ a.u., starting from $t = 0$ a.u. until $t = 0.05$ a.u., the agent receives only the initial state ρ_0 as input and provides signals to control the system's evolution based on the input state. The agent receives the state ρ_1 at $t = 0.05$ a.u., and so on, where at each step, the agent receives the state $\rho_{t-0.05}$, which is the state prior to $\sqcup = 0.05$ a.u.. As shown in the

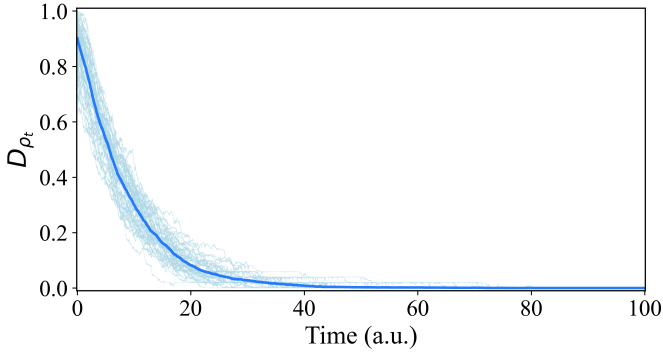


Fig. 7. With a measurement efficiency $\eta_c = 0.8$, under the control of the DRL agent, 50 random initial states stably evolve to the target GHZ state. The light blue lines represent the average evolution trajectories for different initial states, and the dark blue line represents the average trajectory across all different initial states.

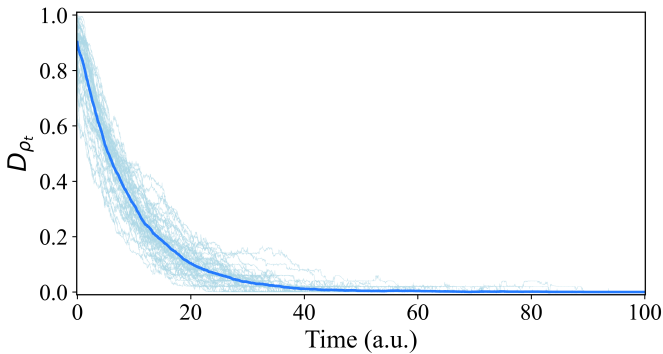


Fig. 8. With a time delay $\Delta = 0.05$ a.u., under the control of the DRL agent, 50 random initial states stably evolve to the target GHZ state. The light blue lines represent the average evolution trajectories for different initial states, and the dark blue line represents the average trajectory across all different initial states.

Figure 8, by selecting 50 different initial states arbitrarily, it can be observed that a well-trained agent still exhibits excellent performance in dealing with time delays, although longer convergence time is required than in the perfect environment in Figure 4.

In order to gain a clear and informative understanding of the impact of time delay on system convergence, the following analysis was conducted:

First, the following assumptions are made:

- It is assumed that the maximum evolution time of the system, denoted as T_{max} , is equal to 100 a.u.. For any evolution, when the system has not converged to the target within the maximum evolution time T_{max} (i.e., when the distance $D_{\rho T_{max}} > 0.001$), it is referred to as a non-convergent trajectory at the maximum evolution time T_{max} .
- A concept of “Stabilization Success Rate” is defined. The objective is to obtain convergence trajectories for 50 different initial states, where each convergence trajectory for an initial state is constructed as an average curve of 50 different trajectories under varying environmental noise. In other words, for 50 different initial states, we have a total of $50 * 50 = 2500$ trajectories. To obtain these 2500

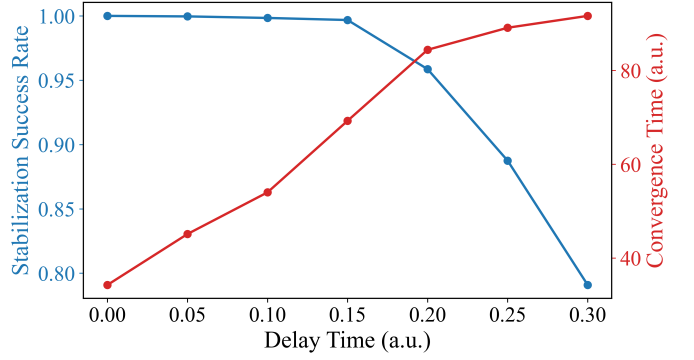


Fig. 9. “Stabilization success rate” (blue) and convergence time (red) with respect to time delay for 50 random initial states stabilized to the target GHZ state under the control of the DRL agent.

trajectories that achieve successful convergence within the time T_{max} , we may need data from more than 2500 trajectories. For instance, when there are 100 non-convergent trajectories, the convergence success rate is calculated as $2500/(2500 + 100) = 0.9615$.

As illustrated in Figure 9, it can be observed that with an increase in time delay, the average time required for the system state to stabilize towards the target increases, while the “Stabilization Success Rate” decreases. For instance, when the time delay is 0.05 a.u., the average convergence time is 38.52 a.u., with a success rate of 0.9913. However, when the time delay is increased to 0.3 a.u., the average convergence time extends to 91.65 a.u., with a corresponding decrease in the success rate to 0.7909. This aligns with common intuition, where a larger time delay leads to poorer performance of the DRL agent.

VI. CONCLUSIONS

In this paper, we designed a DRL agent and applied it to a quantum measurement-based feedback control problem, for stabilizing quantum entangled states. By designing an effective reward function, the trained agent can not only stabilize the quantum system to the target state with high fidelity but also exhibits good robustness. We first tested the well-trained agent in “perfect case” and compared the performance with Lyapunov-based switch method. The results showed that our approach achieves comparable fidelity in shorter time, which has the potential to reduce the interaction between quantum systems with their environment thereby significantly reducing additional noise issues arising from prolonged system-environment interactions. We then tested our agent in different “imperfect cases” including measurement inefficiency and time delay in the feedback loop, where our proposed agent showed good robustness. Lastly, due to the generality of our proposed control framework, extending it to stabilize other quantum states poses minimal challenges. We believe that exploring the behaviors that may exist in real-world environments will be an interesting and challenging research direction. In the future, we will also consider reducing the training time of DRL agents by designing more efficient and faster algorithms.

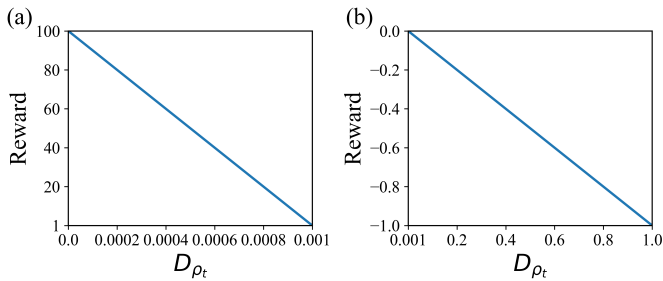


Fig. 10. Linear Reward Function

APPENDIX

THE IMPACT OF DIFFERENT REWARD FUNCTIONS ON AGENT PERFORMANCE

We take the two problems described in Section V (stabilization of 2- and 3-qubit systems) and train our agents using the following three different reward functions to compare their impact on the agents' performance.

- 1) *Sparse Reward*: Only rewards are given when the agent reaches specific states. For example, in games like Go, it is challenging to set rewards for every intermediate move, and the state space is vast, so rewards are only obtained when the final victory is achieved. In our quantum system environment, we can set a reward when the distance $D_{\rho_t} \leq 0.001$. At all other times, the reward is 0.
- 2) *Linear Reward*: As shown in the Figure 10, the system's reward is linearly related to the distance D_{ρ_t} .
- 3) *IPF Reward*: Refer to Section IV-B for details.

To ensure fair comparisons, for a target state, we maintain consistent training parameters for all three agents, with the only difference being the reward functions used during training. Subsequently, we test these trained agents using 50 random initial states. As depicted in Figure 11(a), in the context of the 2-qubit state stabilization problem, agents trained with linear reward (orange) and IPF reward (blue) perform almost identically, both being able to stabilize the system to the desired state within a reasonable time frame. However, the sparse reward function (green) demonstrates a clear inadequacy, as the agent only receives rewards when reaching specific target states, hindering its ability to effectively explore and learn during the training process. Moving on to the more complex 3-qubit system, as shown in Figure (b), the agent trained with the sparse reward function struggle to stabilize the system to the target state. Conversely, the agent trained with the linear reward function exhibit good performance and the ability to reach the target state. However, in comparison to the IPF reward function, the agent guided by the linear reward function lack speed in achieving stability. In contrast, our proposed IPF reward function excels in stabilizing the target state. It provides the agent with balanced guidance, enabling efficient learning and faster convergence to the desired stable states. These highlight the effectiveness and superiority of the IPF reward approach in improving agent performance.

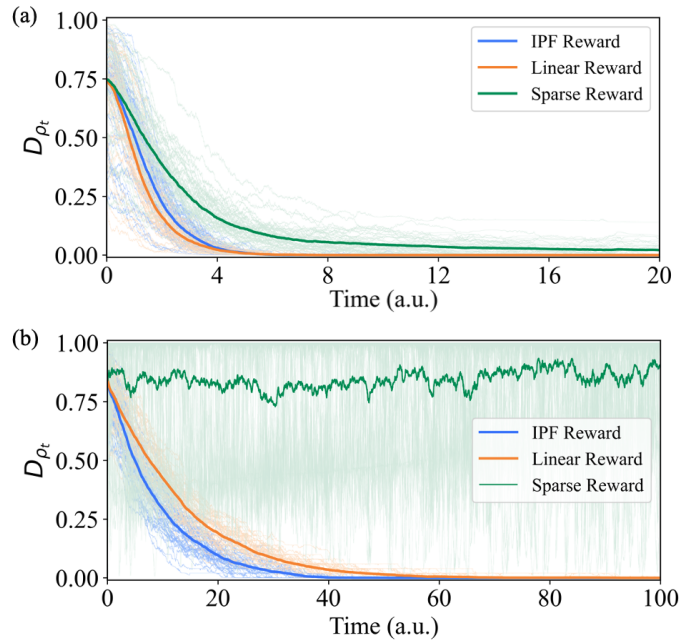


Fig. 11. The performance of agents trained with three different reward functions in (a) two-qubit system (b) three-qubit (GHZ) system.

REFERENCES

- [1] D. Dong and I. R. Petersen, *Learning and Robust Control in Quantum Technology*. Springer Nature, 2023.
- [2] A. Karlsson and M. Bourennane, "Quantum teleportation using three-particle entanglement," *Physical Review A*, vol. 58, no. 6, p. 4394, 1998.
- [3] A. Ekert and R. Jozsa, "Quantum algorithms: entanglement-enhanced information processing," *Philosophical Transactions of the Royal Society of London. Series A: Mathematical, Physical and Engineering Sciences*, vol. 356, no. 1743, pp. 1769–1782, 1998.
- [4] R. Jozsa and N. Linden, "On the role of entanglement in quantum-computational speed-up," *Proceedings of the Royal Society of London. Series A: Mathematical, Physical and Engineering Sciences*, vol. 459, no. 2036, pp. 2011–2032, 2003.
- [5] X. Gu, L. Chen, A. Zeilinger, and M. Krenn, "Quantum experiments and graphs. III. high-dimensional and multiparticle entanglement," *Physical Review A*, vol. 99, no. 3, p. 032338, 2019.
- [6] S. Kuang, D. Dong, and I. R. Petersen, "Rapid Lyapunov control of finite-dimensional quantum systems," *Automatica*, vol. 81, pp. 164–175, 2017.
- [7] Y. Liu, D. Dong, S. Kuang, I. R. Petersen, and H. Yonezawa, "Two-step feedback preparation of entanglement for qubit systems with time delay," *Automatica*, vol. 125, p. 109174, 2021.
- [8] Y. Liu, S. Kuang, and S. Cong, "Lyapunov-based feedback preparation of GHZ entanglement of N -qubit systems," *IEEE Transactions on Cybernetics*, vol. 47, no. 11, pp. 3827–3839, 2016.
- [9] R. S. Judson and H. Rabitz, "Teaching lasers to control molecules," *Physical Review Letters*, vol. 68, no. 10, p. 1500, 1992.
- [10] D. Dong and I. R. Petersen, "Quantum estimation, control and learning: opportunities and challenges," *Annual Reviews in Control*, vol. 54, pp. 243–251, 2022.
- [11] D. Dong, "Learning control of quantum systems," in *Encyclopedia of Systems and Control*, J. Baillieul and T. Samad, Eds. Springer London, 2020, https://doi.org/10.1007/978-1-4471-5102-9_100161-1.
- [12] S. Sharma, H. Singh, and G. G. Balint-Kurti, "Genetic algorithm optimization of laser pulses for molecular quantum state excitation," *The Journal of Chemical Physics*, vol. 132, no. 6, p. 064108, 2010.
- [13] O. M. Shir, *Niching in derandomized evolution strategies and its applications in quantum control*. Leiden University, 2008.
- [14] D. Dong, M. A. Mabrok, I. R. Petersen, B. Qi, C. Chen, and H. Rabitz, "Sampling-based learning control for quantum systems with uncertainties," *IEEE Transactions on Control Systems Technology*, vol. 23, no. 6, pp. 2155–2166, 2015.
- [15] H. M. Wiseman, "Quantum theory of continuous feedback," *Physical Review A*, vol. 49, no. 3, p. 2133, 1994.

- [16] V. Mnih, K. Kavukcuoglu, D. Silver, A. Graves, I. Antonoglou, D. Wierstra, and M. Riedmiller, "Playing atari with deep reinforcement learning," *arXiv preprint arXiv:1312.5602*, 2013.
- [17] D. Silver, A. Huang, C. J. Maddison, A. Guez, L. Sifre, G. Van Den Driessche, J. Schrittwieser, I. Antonoglou, V. Panneershelvam, M. Lanctot *et al.*, "Mastering the game of Go with deep neural networks and tree search," *Nature*, vol. 529, no. 7587, pp. 484–489, 2016.
- [18] C. Chen, D. Dong, H.-X. Li, J. Chu, and T.-J. Tarn, "Fidelity-based probabilistic Q-learning for control of quantum systems," *IEEE Transactions on Neural Networks and Learning Systems*, vol. 25, no. 5, pp. 920–933, 2013.
- [19] H. Ma, D. Dong, S. X. Ding, and C. Chen, "Curriculum-based deep reinforcement learning for quantum control," *IEEE Transactions on Neural Networks and Learning Systems*, vol. 34, no. 11, pp. 8852–8865, 2023.
- [20] R. Porotti, A. Essig, B. Huard, and F. Marquardt, "Deep reinforcement learning for quantum state preparation with weak nonlinear measurements," *Quantum*, vol. 6, p. 747, 2022.
- [21] A. Perret and Y. Bérubé-Lauzière, "Preparation of cavity-Fock-state superpositions by reinforcement learning exploiting measurement back-action," *Physical Review A*, vol. 109, no. 2, p. 022609, 2024.
- [22] V. Sivak, A. Eickbusch, H. Liu, B. Royer, I. Tsoutsios, and M. Devoret, "Model-free quantum control with reinforcement learning," *Physical Review X*, vol. 12, no. 1, p. 011059, 2022.
- [23] M. Y. Niu, S. Boixo, V. N. Smelyanskiy, and H. Neven, "Universal quantum control through deep reinforcement learning," *npj Quantum Information*, vol. 5, no. 1, p. 33, 2019.
- [24] Z. T. Wang, Y. Ashida, and M. Ueda, "Deep reinforcement learning control of quantum cartpoles," *Physical Review Letters*, vol. 125, no. 10, p. 100401, 2020.
- [25] S. Borah, B. Sarma, M. Kewming, G. J. Milburn, and J. Twamley, "Measurement-based feedback quantum control with deep reinforcement learning for a double-well nonlinear potential," *Physical Review Letters*, vol. 127, no. 19, p. 190403, 2021.
- [26] A. C. Doherty, S. Habib, K. Jacobs, H. Mabuchi, and S. M. Tan, "Quantum feedback control and classical control theory," *Physical Review A*, vol. 62, no. 1, p. 012105, 2000.
- [27] K. Jacobs and D. A. Steck, "A straightforward introduction to continuous quantum measurement," *Contemporary Physics*, vol. 47, no. 5, pp. 279–303, 2006.
- [28] H. M. Wiseman and G. J. Milburn, *Quantum Measurement and Control*. Cambridge University Press, 2009.
- [29] M. Van Otterlo and M. Wiering, "Reinforcement learning and Markov decision processes," *Reinforcement Learning: State-of-the-Art*, pp. 3–42, 2012.
- [30] B. Qi, Z. Hou, L. Li, D. Dong, G. Xiang, and G. Guo, "Quantum state tomography via linear regression estimation," *Scientific Reports*, vol. 3, no. 1, p. 3496, 2013.
- [31] J. A. Smolin, J. M. Gambetta, and G. Smith, "Efficient method for computing the maximum-likelihood quantum state from measurements with additive gaussian noise," *Physical Review Letters*, vol. 108, no. 7, p. 070502, 2012.
- [32] V. Mnih, K. Kavukcuoglu, D. Silver, A. A. Rusu, J. Veness, M. G. Bellemare, A. Graves, M. Riedmiller, A. K. Fidjeland, G. Ostrovski *et al.*, "Human-level control through deep reinforcement learning," *Nature*, vol. 518, no. 7540, pp. 529–533, 2015.
- [33] R. S. Sutton, D. McAllester, S. Singh, and Y. Mansour, "Policy gradient methods for reinforcement learning with function approximation," *Advances in Neural Information Processing Systems*, vol. 12, 1999.
- [34] V. Konda and J. Tsitsiklis, "Actor-critic algorithms," *Advances in Neural Information Processing Systems*, vol. 12, 1999.
- [35] J. Schulman, F. Wolski, P. Dhariwal, A. Radford, and O. Klimov, "Proximal policy optimization algorithms," *arXiv preprint arXiv:1707.06347*, 2017.
- [36] F. Pardo, A. Tavakoli, V. Levdik, and P. Kormushev, "Time limits in reinforcement learning," in *Proceedings of the 35th International Conference on Machine Learning*, ser. Proceedings of Machine Learning Research, J. Dy and A. Krause, Eds., vol. 80. PMLR, 10–15 Jul 2018, pp. 4045–4054.
- [37] M. Riedmiller, R. Hafner, T. Lampe, M. Neunert, J. Degraeve, T. van de Wiele, V. Mnih, N. Heess, and J. T. Springenberg, "Learning by playing solving sparse reward tasks from scratch," in *Proceedings of the 35th International Conference on Machine Learning*, ser. Proceedings of Machine Learning Research, J. Dy and A. Krause, Eds., vol. 80. PMLR, 10–15 Jul 2018, pp. 4344–4353.
- [38] D. Hadfield-Menell, S. Milli, P. Abbeel, S. J. Russell, and A. Dragan, "Inverse reward design," *Advances in Neural Information Processing Systems*, vol. 30, 2017.
- [39] T. Xie, Y. Ma, and Y.-X. Wang, "Towards optimal off-policy evaluation for reinforcement learning with marginalized importance sampling," *Advances in Neural Information Processing Systems*, vol. 32, 2019.
- [40] A. Raffin, A. Hill, A. Gleave, A. Kanervisto, M. Ernestus, and N. Dornmann, "Stable-baselines3: Reliable reinforcement learning implementations," *Journal of Machine Learning Research*, vol. 22, no. 268, pp. 1–8, 2021.
- [41] M. Towers, J. K. Terry, A. Kwiatkowski, J. U. Balis, G. d. Cola, T. Deleu, M. Goulão, A. Kallinteris, A. KG, M. Krimmel, R. Perez-Vicente, A. Pierré, S. Schulhoff, J. J. Tai, A. T. J. Shen, and O. G. Younis, "Gymnasium," Mar. 2023.
- [42] R. S. Sutton and A. G. Barto, *Reinforcement learning: An introduction*. MIT press, 2018.
- [43] J. Schulman, P. Moritz, S. Levine, M. Jordan, and P. Abbeel, "High-dimensional continuous control using generalized advantage estimation," *arXiv preprint arXiv:1506.02438*, 2015.
- [44] X. B. Peng, P. Abbeel, S. Levine, and M. Van de Panne, "Deepmimic: Example-guided deep reinforcement learning of physics-based character skills," *ACM Transactions on Graphics (TOG)*, vol. 37, no. 4, pp. 1–14, 2018.
- [45] M. Mirrahimi and R. van Handel, "Stabilizing feedback controls for quantum systems," *SIAM Journal on Control and Optimization*, vol. 46, no. 2, pp. 445–467, 2007.
- [46] D. M. Greenberger, M. A. Horne, and A. Zeilinger, "Going beyond bell's theorem," in *Bell's theorem, quantum theory and conceptions of the universe*. Springer, 1989, pp. 69–72.
- [47] W. Dür, G. Vidal, and J. I. Cirac, "Three qubits can be entangled in two inequivalent ways," *Physical Review A*, vol. 62, no. 6, p. 062314, 2000.
- [48] T. Monz, P. Schindler, J. T. Barreiro, M. Chwalla, D. Nigg, W. A. Coish, M. Harlander, W. Hänsel, M. Hennrich, and R. Blatt, "14-qubit entanglement: Creation and coherence," *Physical Review Letters*, vol. 106, no. 13, p. 130506, 2011.
- [49] S. Kuang, G. Li, Y. Liu, X. Sun, and S. Cong, "Rapid feedback stabilization of quantum systems with application to preparation of multiqubit entangled states," *IEEE Transactions on Cybernetics*, vol. 52, no. 10, pp. 11 213–11 225, 2021.
- [50] J. Zhang, Y.-x. Liu, R.-B. Wu, K. Jacobs, and F. Nori, "Quantum feedback: theory, experiments, and applications," *Physics Reports*, vol. 679, pp. 1–60, 2017.